SCATTERING OF LAMB WAVES IN A COMPOSITE PLATE

Robert Bratton and Subhendu Datta

Department of Mechanical Engineering
University of Colorado
Campus Box 427
Boulder, CO 80302

Arvind Shah

Department of Civil Engineering
University of Manitoba
Winnipeg, Manitoba
Canada R3T 2N2

INTRODUCTION

Recent investigations of space construction techniques have explored the use of composite materials in the construction of space stations and platforms. These composites offer superior strength to weight ratio and are thermally stable. Examples of these materials are laminates of graphite fibers in an epoxy or a metal(Al, Mg) matrix and boron fibers in an aluminum matrix. The overall effective elastic constants of such a medium can be calculated from fiber and matrix properties by using an effective modulus theory as shown in [1] and [2]. The investigation of propagation and scattering of elastic waves in composite materials is necessary in order to develop an ability to characterize cracks and predict the reliability of composite structures. The objective of this investigation is the characterization of a surface breaking crack by ultrasonic techniques. In particular, the use of Lamb waves for this purpose is studied here. The Lamb waves travel through the plate, encountering a crack, and scatter. Of interest is the modeling of the scattered wave in terms of the Lamb wave modes.The direct problem of propagation and scattering of Lamb waves by a surface breaking crack has been analyzed. This would permit an experimentalist to characterize the crack by comparing the measured response to the analytical model.The plate is assumed to be infinite in the x and y directions with a constant thickness in the z direction. The top and bottom surfaces are traction free. Solving the governing wave equations and using the stress-free boundary conditions results in the dispersion equation. This equation yields the guided modes in the homogeneous plate. The theoretical model is a hybrid method that combines analytical and finite elements techniques to describe the scattered displacements. A finite region containing the defects is discretized by finite elements. Outside the local region, the far field solution is expressed as a Fourier summation of the guided modes obtained from the dispersion equation. Continuity of tractions and displacements at the boundaries of the two regions provides the necessary equations to determine the expansion coefficients and the nodal displacements. This method was used for out-of-plane(SH) wave scattering in an isotropic plate[3]. A combined analytical and finite element formulation for a single layered isotropic plate in the state of plane strain was investigated in [4]. In this study the authors considered only the lowest symmetric mode and geometrically symmetric cracks. In [5] a variational approach was used to investigate scattering by a symmetric

Review of Progress in Quantitative Nondestructive Evaluation, Vol. 10B
Edited by D.O. Thompson and D.E. Chimenti, Plenum Press, New York, 1991

pair of surface breaking thin slots. Employing standard elastostatic crack solutions as trial functions the authors examined the scattering by the first symmetric mode. A finite difference method was used in [6] to calculate the scattering of Lamb and shear waves from surface breaking cracks. In [7] a modified Wiener-Hopf technique was used to analyze scattering of Lamb waves by a crack. Applying this technique, the authors in [8] studied quantitative sizing of spot welds in joined sheets. Besides the finite difference and finite element techniques, the analytical approaches are not suitable for analyzing arbitrarily shaped defects and anistropic media. In the hybrid method used here these defects can be of arbitrary shapes as well as inclusions of different material. Recently, using the hybrid method, the scattering by surface-breaking cracks in isotropic homogeneous and welded plates has been examined in [9].

HYBRID MODELING

As explained in the Introduction the objective of this research is to model ultrasonic techniques for characterization of defects in composite plates. The particular ultrasonic technique explored here is based on the modal representation. Flaw size, orientation, and location in the plate all influence plate mode interaction. This has the possibility that detailed analysis of the modal signature will yield information on flaw character. The guided or Lamb modes being considered here are two dimensional. When the incident wave travels parallel or perpendicular to the axis of symmetry(parallel to the fibers) the SH modes decouple from these modes. This situation will be assumed in this work. The plate being modeled in this investigation is shown in Fig. 1 and is taken to be of uniform thickness H with traction free surfaces. All the inclusions or inhomogeneities are assumed to be in the interior region bounded by the vertical boundaries at $x=x_{right}$ and $x=-x_{left}$. The incident wave studied here may travel in the $\pm$ x directions. The particle motion of interest is in the xz plane. The time factor $e^{-i\omega t}$ is dropped from all the following expressions. The total displacement at the boundaries is the sum of the incident and scattered displacements

$$U = U^i + U^s \tag{1}$$

where, U^i denotes the incident field and U^s represents the scattered field. The superscripts i and s denote incident and scattered fields, respectively. The incident field is taken as a single mode of order m traveling in the positive x direction written in the following form,

$$U^i = A_m U_m(z) e^{ik_m x} \tag{2}$$

where k_m is the wavenumber of the incident mode at a given frequency, A_m is the amplitude of the wave, and $U_m(z)$ is the mode shape function that varies through the thickness of the plate.

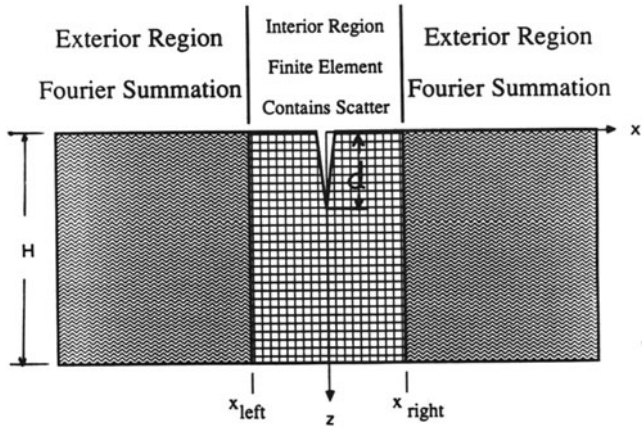

Fig. 1. Geometry of the plate in the hybrid method

This vector contains the displacement components in the x and z directions. The exterior scattered field is approximated by superposition of a finite number of Lamb modes. These modes are either propagating, nonpropagating or evanescent in the negative and positive x directions. This can be expressed by the following summation of M modes:

$$\boldsymbol{U}^{s+}(x,z) = \sum_{n=1}^{M} B_n^{+} \boldsymbol{U}_n^{+}(z) e^{ik_n x}, \quad x \geq x_R \tag{3}$$

$$\boldsymbol{U}^{s-}(x,z) = \sum_{n=1}^{M} B_n^{-} \boldsymbol{U}_n^{-}(z) e^{-ik_n x}, \quad x \leq -x_L \tag{4}$$

where B_n^{+} and B_n^{-} are undetermined amplitudes of the nth mode of the scattered field. $\boldsymbol{U}_n^{\pm}(z)$ represents the displacement vector through the thickness of the plate containing the x and z components. The superscript $\pm$ denotes positive or negative x sides of the interior region(minus for left and plus for the right). The wavenumbers of the modes for a given frequency are found using the method described in [10]. The column vector $\boldsymbol{U}_n^{\pm}(z)$ is evaluated at each nodal location. The expressions for the x and z components of $\boldsymbol{U}_n^{\pm}$ will be denoted by the symbols u and w, respectively. These can be found in [11]. The plate is divided into N layers with N+1 nodes on the right and left boundaries. Equations (3) and (4) can be written in matrix form as

$$\{\boldsymbol{U}^{s-}\} = [G^{-}]\{B^{-}\}, \quad x \leq -x_L \tag{5}$$

$$\{\boldsymbol{U}^{s+}\} = [G^{+}]\{B^{+}\}, \quad x \geq x_R \tag{6}$$

where the matrix $[G^{\pm}]$ is defined as having M columns of the vector $\boldsymbol{U}_n^{\pm}(z)$ whose 2(N+1) elements correspond to the x and z components of the displacement at each nodal location. The column matrices $\{B^{-}\}$ and $\{B^{-}\}$ defined as

$$\left\{B_1^{-}e^{-ik_1x}\ B_2^{-}e^{-ik_2x}\ \cdots\ B_M^{-}e^{-ik_Mx}\right\}^T \quad , \quad \left\{B_1^{+}e^{ik_1x}\ B_2^{+}e^{ik_2x}\ \cdots\ B_M^{+}e^{ik_Mx}\right\}^T. \tag{7}$$

In the above equations, the number of rows(twice the number of nodes on a vertical boundary) and the number of columns(the number of modes in the Fourier summation) do not have to be equal. In fact, it would be advantageous if the number of modes is smaller than the number of degrees of freedom on a vertical boundary, thereby reducing the storage requirements for [G]. The number of modes used in the summation must include all the propagating modes and a certain number of imaginary and complex branches. Expanding Eq. (1) in terms of the incident wave contributions, Eq. (2), and the far field expansion, Eqs. (5), and (6), yields expressions for the total displacements at the nodal locations for an arbitrary x location,

$$\{U^{+}\} = [G^{+}]\{A_m\delta_{mn}e^{ik_nx}\} + [G^{+}]\{B_n^{+}e^{ik_nx}\}, \quad x \geq x_R \tag{8}$$

$$\{U^{-}\} = [G^{+}]\{A_m\delta_{mn}e^{ik_nx}\} + [G^{-}]\{B_n^{-}e^{-ik_nx}\}, \quad x \leq -x_L. \tag{9}$$

The displacements field in the interior region is represented by finite elements. The variational principle is used to form an impedance matrix [S] = [K]-ω^2[M] relating the total displacements to the imposed forces at the nodes of the boundaries of the finite element mesh. Assembling the elements, the equations governing the interior and boundary displacements can be written in the following form:

$$\begin{bmatrix} S_{LL} & S_{LI} & S_{LR} \\ S_{IL} & S_{II} & S_{IR} \\ S_{RL} & S_{RI} & S_{RR} \end{bmatrix} \begin{bmatrix} U_L^- \\ U_I \\ U_R^+ \end{bmatrix} = \begin{bmatrix} F_B^- \\ 0 \\ F_B^+ \end{bmatrix}. \tag{10}$$

The displacements U_L, U_I, and U_R are nodal displacements on the left boundary, in the interior region, and on the right boundary, respectively. F_B^- and F_B^+ stand for the interaction forces on the left and right boundaries due to the incident and scattered fields. Since there are no nodes connecting the left and right boundaries, $S_{RL}=S_{LR}=0$. At each nodal location on the boundaries, the vectors F_B^+ and F_B^- can be constructed using the modal representation of the displacements. These forces can be described by incident and scattered modes as

$$\{F_B^+\} = [F^+]\{A_m\delta_{mn}e^{ik_nx}\} + [F^+]\{B_n^+e^{ik_nx}\}, \qquad x \geq x_R \tag{11}$$

$$\{F_B^-\} = -[F^+]\{A_m\delta_{mn}e^{ik_nx}\} - [F^-]\{B_n^-e^{-ik_nx}\}, \qquad x \leq -x_L. \tag{12}$$

The matrices $[F^{\pm}]$ are constructed in a similar fashion as the $[G^{\pm}]$. The negative signs in Eq. (12) are the resultant of the dot product of the normal on the left boundary. Combining Eqs. (8) and (9) with Eqs. (11) and (12) allows the expressions for $\{F_B^+\}$ and $\{F_B^-\}$ to be written in terms of known incident field contributions and the unknown displacements $\{U^{\pm}\}$. Using these expressions for $\{F_B^+\}$ and $\{F_B^-\}$ in Eq. (10) and moving the unknown terms to the left side of the equality a modified impedance matrix is formed. Using a banded solver the total displacements can be obtained and subsequently, the $B_n^{\pm}$ coefficients can be determined from Eqs. (8) and (9). Having obtained the coefficients $B_n^{\pm}$, the reflection and transmission coefficients can be determined by the following relations,

$$R_{mn} = \frac{B_n^-}{A_m}$$

$$T_{mn} = \frac{B_n^+}{A_m}, \; n \neq m, \qquad T_{mm} = 1 + \frac{B_m^+}{A_m}. \tag{13}$$

The subscripts m,n are indices denoting the coefficients of the nth scattered mode due to the mth incident mode. The method outlined above was applied to an uniaxial graphite/epoxy plate with a dimensionless thickness of 1. The reflection and transmission coefficients were obtained for a normal surface breaking crack. The surface breaking crack requires both symmetric and anti-symmetric modes in the Fourier summation. This is due to the fact that if a symmetric mode is incident, then the scattered modes are composed of both symmetric and anti-symmetric modes. The crack is modeled as a traction-free infinitesimally thin notch. The upper limit of the dimensionless frequency investigated corresponds to the second symmetric cutoff frequency. The number of modes, M, used was 30 to 33. As shown in the dispresion curve of Fig. 2, the number of nonpropagating and evanescent modes vary as one increases the frequency. When the largest evanescent mode was selected all nonpropagating modes having the wavenumber less than or equal to the imaginary part of the wavenumber of the evanescent mode were included. Included also in the summation was the evanescent mode with the same imaginary part of the wavenumber but with the real negative part. The nondimensional form of the frequency and wavenumber are used in Fig. 2 and are defined as $\Omega = \frac{\omega H}{2\pi\sqrt{C_{55}/\rho}}$ and $K = kH/2\pi$.

SURFACE CRACK PROBLEM

In this section results will be presented showing the behavior of the transmission and reflection coefficients for a normal surface breaking crack.To be useful for ultrasonic NDE applications it is necessary to have the transmission and reflections coefficients as functions of

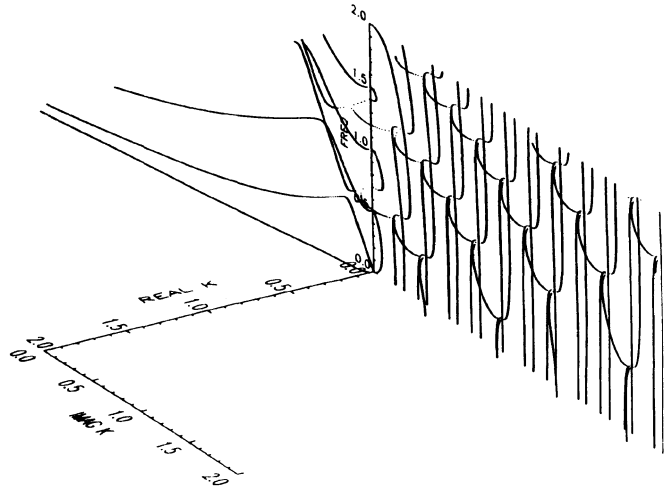

Fig. 2. Dispersion curve of the graphite/epoxy plate from [11]

the frequency for a constant value of d/H. Two values of d/H were chosen 0.3 and 0.6. In figures 3(a) and 3(b), the magnitudes of the reflection and transmission coefficients are shown as functions of the nondimensional frequency, Ω. The open triangles denote the actual calculated data points, while the lines represent cubic spline approximations. As seen in these figures the behavior is quite dramatic for d/H = 0.6 and much less so for 0.3. In Fig. 3(a) at the first antisymmetric cutoff frequency of 0.5, sharp discontinuities in the slopes are seen for the crack-depth d/H = 0.6. The reduction in the transmission coefficient and the increase in the reflection coefficient seem to indicate a behavior that may be exploited for ultrasonic characterization of this crack. For the crack-depth, d/H = 0.3, the magnitudes of the coefficients in Fig. 3(b) show similar behavior and thus should help in ultrasonic characterization at Ω=0.5. In the same figure at the second symmetric mode(S_1) cutoff frequency(Ω=0.7) the transmission coefficient approaches 1.0 and the reflection coefficient is nearly zero. This behavior suggests that the incident mode does not interact with the crack and near this frequency the sensitivity will be lost. It is expected that this analysis at lower frequencies will allow more detailed knowledge of the individual modal contributions to the total response. As the number of modes increases with increasing frequency, the interpretation becomes more difficult. It is expected that using lower frequencies and thereby reducing the number of modes being scattered will improve the interpretability of the transmitted and reflected signals.

TIME RESPONSE OF A PLATE WITH A CRACK

The interaction of elastic waves with defects and subsequent echoes provide an indication of the presence of the defect and with further analysis the size of the defect. The frequency response was constructed by using the modal response due to a vertical load and the transmission coefficient $T_{mm}(\omega)$. This was then inverted by an inverse FFT algorithm to get the time response of the graphite/epoxy plate with a normal surface breaking crack. The incident field will be expressed as a summation over discrete frequencies:

$$U^I = \sum_{j=1}^{J} A_j(\omega_j) \sum_{n=1}^{N_j} U_n e^{ik_n x}. \tag{14}$$

where J is the number of frequencies used in the discretization of the forcing function, j is the index for frequencies, N_j is the number of modes for each frequency, n is the index for modes, A_j is the amplitude of the Gaussian beam at the value of ω_j, k_n is the nth wavenumber at the

frequency ω_j, and $U_n e^{ik_n x}$ is the eigenmode vector corresponding to the nth wavenumber. Equation (14) describes the motion of a point of the plate by a discrete set of eigenmodes. These eigenmodes result from the evaluation at discrete frequencies of the Fourier transform with respect to time of the Green's function for the plate. The Green's function describes the response of the plate due to a normal line load with an impulsive time dependence. Note that Eq. (14) is applicable for any type of transducers with a known amplitude spectrum. Evaluating Eq. (14) by an inverse fast Fourier transform(FFT) algorithm, the time trace at the receiver can be obtained for a plate without a crack. To obtain the time trace with a crack Eq. (14) is modified to include the scattered modes. The modified equation (14) is defined as

$$U^R = \sum_{j=1}^{J} A_j(\omega_j) \sum_{m=1}^{N_j} \sum_{n=1}^{N_j} R_{mn}(\omega_j) U_n e^{ik_n x}$$

$$U^T = \sum_{j=1}^{J} A_j(\omega_j) \sum_{m=1}^{N_j} \sum_{n=1}^{N_j} T_{mn}(\omega_j) U_n e^{ik_n x} \qquad (15)$$

where the index m stands for the incident mode and the index n stands for the converted mode.

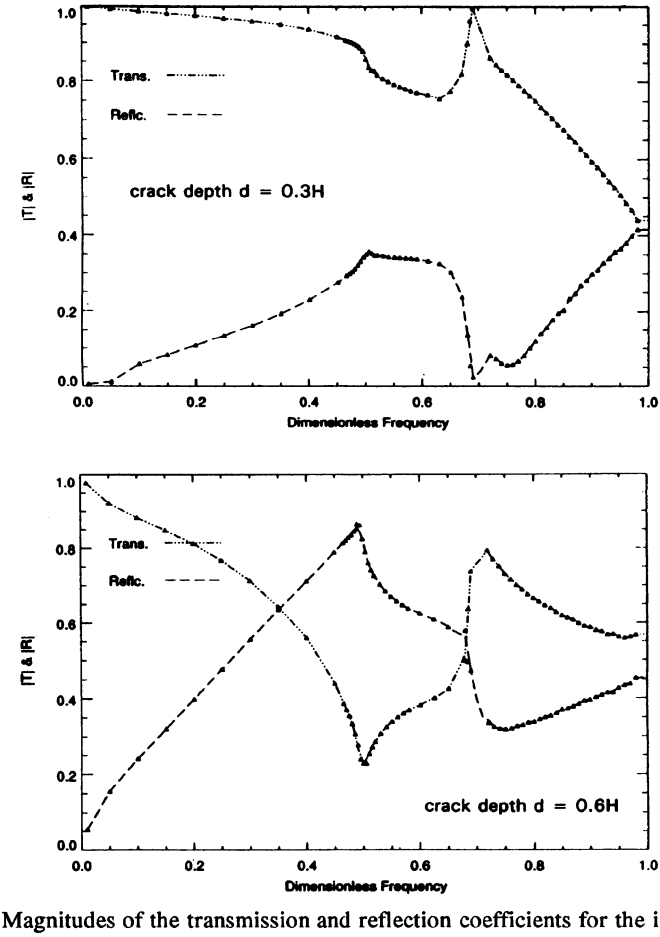

Fig. 3. Magnitudes of the transmission and reflection coefficients for the incident S_0 mode versus dimensionless frequency for the crack depths of (a) d=0.3H and (b) d=0.6H

Again using an inverse FFT algorithm and Eq. (15) the time trace can be obtained for a plate with a crack. This procedure was adopted for the incident S_0 mode(i.e., $N_m=1$) for a 1 mm thick graphite/epoxy plate. The properties of the plate are given in Table 1. The Gaussian pulse representing the frequency dependence of the transducer was centered at 1 MHz($\Omega=0.5$) in order to capture the behavior of the transmission coefficient at the frequency of the A_1 mode cutoff as seen in Figs. 3(a)-(b). The bandwidth of the pulse was approximately 2 kHz. Beyond this the pulse amplitude is negligible. This type of pulse results in a highly oscillatory time signal. This required the frequency range over which the signal is sampled to be extended to 4 MHz. The number of frequencies sampled was 4096. The resulting time traces for the x-component of the symmetric motion are shown in figures 4(a) and 4(b). The two time traces for the surface

TABLE 1. Material properties for the graphite/epoxy plate

Stiffnesses in 10^{11} N/m^2; density in g/cm^3

C_{11}	C_{33}	C_{12}	C_{55}	ρ
1.6073	0.1392	0.0644	0.0707	1.8

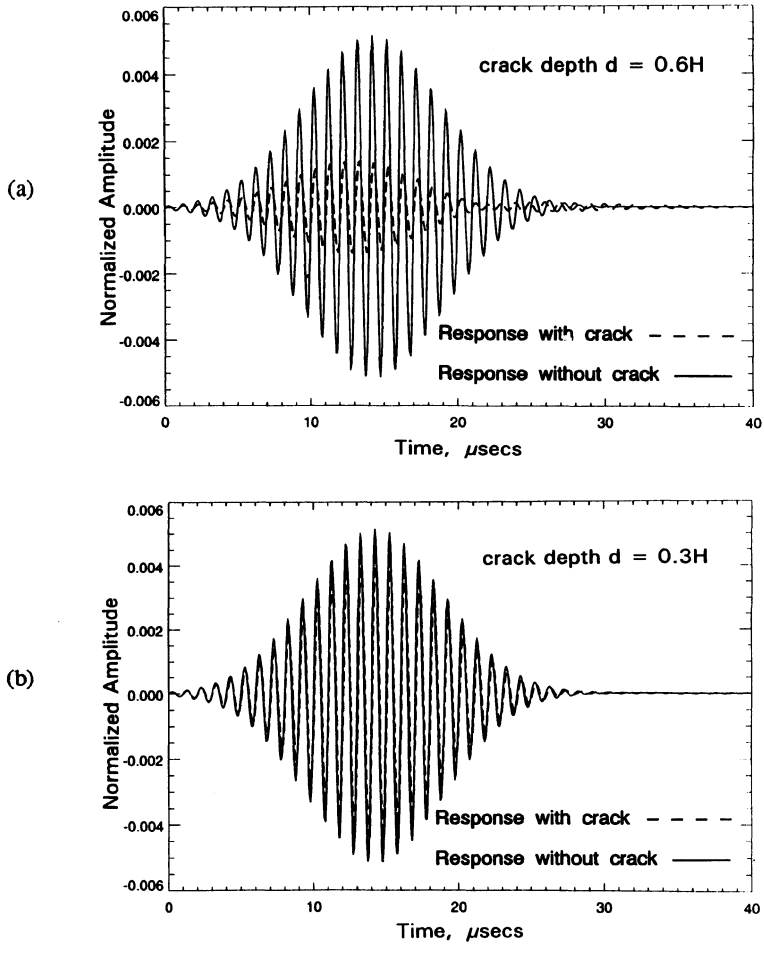

Fig. 4. Time traces for a graphite/epoxy plate with cracks of depths (a) 0.6H and (b) 0.3H

breaking crack clearly show the influence of the crack depth on the reduction in the amplitude of the signal. In these figures the abscissa shows the time in μsecs and the ordinate the normalized amplitude(normalized to the thickness of the plate). The solid line is the time trace at the receiver without the crack and the dashed line the time trace with the crack. In both figures fairly small phase shifts are seen. Comparison of the highest amplitudes do not show any simple relationship between the crack-depth and reduction in the amplitude. With only two crack-depths investigated it is difficult to make any conclusions on the relationship between the crack-depth and the reduction of the amplitude. However, these results clearly show the influence of increasing crack lengths. Further study would provide the means of determining the crack-depth from the scattered signal.

CONCLUSIONS

In order to gain a better understanding of the scattering of elastic waves by defects a combined analytical and finite element technique was developed. The hybrid method is capable of predicting scattered displacements from arbitrary shaped defects as well as inclusions of different material. The defects were contained in a finite region discretized by finite elements. Outside the local region, the far field solution was expressed as a Fourier summation of the guided modes obtained from the dispersion equation. The continuity of traction and displacements at the boundaries of the two regions provided the necessary equations to determine the expansion coefficients and nodal displacements. Although no simple relationship was found between the reduction of the amplitudes and the depths of the cracks, the results clearly show the influence of increasing crack depth on the scattered signal.

ACKNOWLEDGEMENT

The work reported here was supported in part by the Office of Naval Research under Grant N000014-86-K-0280, by the National Aeronautics and Space Administration (Grant NAGW-1388), and from the Natural Science and Engineering Research Council of Canada (Grant OGP-0007988).

REFERENCES

1. S. K. Datta, H. M. Ledbetter, and R. Kriz, Int. J. Solids Struct. 20, 429 (1984).
2. H. M. Ledbetter, S. K. Datta, and T. Kyono, J. Appl. Phys. 65 3411 (1989).
3. Z. Abduljabbar, S. K. Datta, and A. H. Shah, J. Appl. Phys. 20, 461 (1984).
4. M. Koshiba, S. Karakida, and M. Suzuki, IEEE Transactions on Sonics and Ultrasonics SU-31, 18 (1984).
5. B. A. Auld, and M. Tan, 1977 Ultrasonics Symposium Proceedings, p. 61 (1977).
6. A. H. Harker, J. of Nondestructive Evaluation 4 89 (1984).
7. S. I. Rokhlin, J. Acoust. Soc. Am. 67 1157 (1980).
8. F. Bendec, M. Peretz, and S. I. Rokhlin, Ultrasonics, March, 78 (1984).
9. Y. Al-Nassar, Ph.D. dissertation, University of Colorado, 1990 (unpublished).
10. S. K. Datta, A. H. Shah, R. L. Bratton, and T. Chakarborty, J. Acoust. Soc. Am. 83, 2020 (1988b).
11. R. L. Bratton, S. K. Datta, and A. H. Shah, University of Colorado, Center for Space Construction, Report No. 90-1.